ADVANCED FUNCTIONAL MATERIALS
www.afm-journal.de

Cost-Effective Bilayer Radiative Cooling Paint via a Porous P(VDF-HFP) Top Layer

Qilong Cheng, Chao Tang, Byung-Wook Kim, Yuan Xu, Nanfang Yu, Jyotirmoy Mandal, Huiming Yin, and Yuan Yang**

Global warming has led to an increasing demand for cooling solutions, but traditional cooling technologies consume more electricity and increase carbon emissions. Radiative cooling has emerged as a promising alternative, offering sustainable cooling without electricity consumption. Over the past decade, various material designs have demonstrated radiative cooling performance. Particularly, fluoropolymer-based radiative cooling paints stand out as a practical solution, offering ease of application and scalability. However, its cost is ≈5 times of conventional acrylic paints. By understanding the dependence of reflectance on light wavelength, this study proposes a cost-effective bilayer polymer design with attractive cooling performance. The top porous P(VDF-HFP) layer is effective enough to reflect UV and blue light in the solar spectrum and enhance solar stability while reducing the material usage by ≈70%, and the bottom commercial acrylic latex paint reflects the rest of the solar spectrum. This bilayer paint synergistically exhibits relatively high solar reflectance (≈0.9), moderate material cost (≈$1.3 m^{-2}), and excellent UV durability (11 years equivalent). This innovative design achieves a balance between optical performance and economic efficiency, making it a viable candidate for real-world massive implementation of radiative cooling solutions across various applications.

1. Introduction

The world is experiencing an unprecedented temperature rise due to global warming, driving a rapid increase in cooling demand. As extreme heat events become more frequent,[1] the need for air conditioning and other cooling solutions has surged, particularly in developing regions.[2] However, traditional cooling technologies, such as refrigeration compressors, face the "air conditioning paradox"[3] their operation relies on fossil fuels, which in turn amplifies carbon emissions and accelerates climate change. To address this dilemma, researchers are exploring innovative solutions, with radiative cooling emerging as a promising alternative clean technology.[4] This method cools surfaces by emitting thermal radiation through the 7–14 μm atmospheric transparent window to the 3 K outer space as a natural heat sink without consuming any electricity, offering a potential pathway to sustainable cooling in such a warming world.

Over the past decade, multiple material designs have been proposed to successfully demonstrate radiative cooling performance, including multilayer photonic structures,[4,5] porous polymers,[6–8] cellulose derivatives,[9,10] ceramics,[11–13] and more. Additionally, nonreciprocal thermal materials, which violate Kirchhoff's law, have introduced new possibilities for radiative cooling, but they do not seem to enhance cooling performance.[14] Although various types of materials have been developed with demonstrated cooling potentials, significant challenges remain for large-scale implementation in real-world scenarios.[15] For instance, photonic materials are typically fabricated through thin-film deposition or lithography, requiring sophisticated equipment and processes, which presents a limit to be only fabricated in factories. Solar-reflective cooling wood is manufactured by removing color-causing components (e.g., lignin) through chemical treatment[9]—a process that is both time-consuming and energy-intensive. Recently developed cooling ceramics also rely on high-temperature sintering processes.[11,12]

Among these approaches, paints stand out as the most practical and effective choice for large-scale applications,[16] as their implementation does not require the aforementioned energy-intensive processing but instead involves simple spray coating or brush painting. Furthermore, ongoing research into cost-effective paint formulations[16–18] is actively addressing scalability challenges, positioning radiative cooling paints to be deeply linked with Sustainable Development Goals (SDGs) for reducing

Q. Cheng, Y. Xu, N. Yu, Y. Yang
Department of Applied Physics and Applied Mathematics
Columbia University
New York, NY 10027, USA
E-mail: qc2314@columbia.edu; yy2664@columbia.edu
C. Tang
Department of Mechanical Engineering
Columbia University
New York, NY 10027, USA
B.-W. Kim, H. Yin
Department of Civil Engineering and Engineering Mechanics
Columbia University
New York, NY 10027, USA
J. Mandal
Department of Civil and Environmental Engineering
Princeton University
Princeton, NJ 08544, USA
The ORCID identification number(s) for the author(s) of this article can be found under https://doi.org/10.1002/adfm.202506405

DOI: 10.1002/adfm.202506405

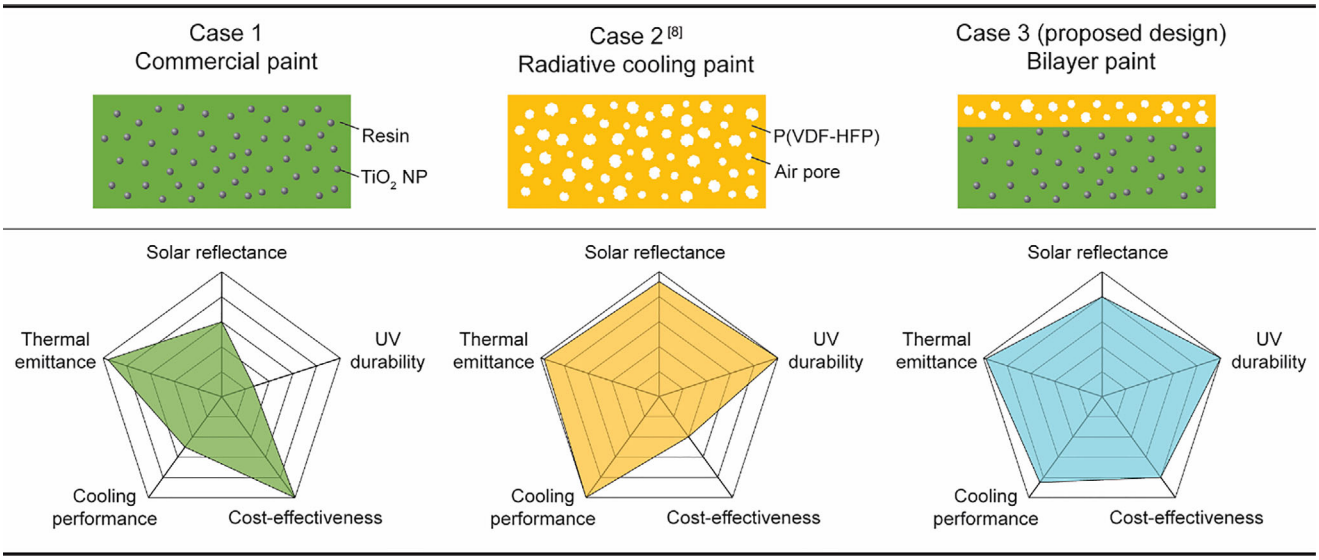

Figure 1. Typical polymer paints as radiative cooling coatings[8] include three cases comparing the optical properties, cost, and performance. The proposed bilayer paint (Case 3) demonstrates relatively high cooling performance, moderate material cost, and excellent UV durability.

building energy consumption and mitigating global warming: SDG 7 of "Affordable and Clean Energy", SDG 11 of "Sustainable Cities and Communities", and SDG 13 of "Climate Action".[19–21] However, balancing performance, durability, and cost remains a critical hurdle. Achieving optimal cooling efficiency while ensuring long-lasting durability under various environmental conditions is essential for these paints to reach widespread adoption and maximize their environmental impact.

Paints offer distinct advantages in terms of ease of application, scalability, and cost-effectiveness compared to more complex photonic structures or thin films. Specifically, **Figure 1** compares several polymer-based paints. Current commercial high-reflective white paint (Case 1), costing ≈\$0.5 m^{-2}, achieves only a solar reflectance of ≈0.8 at a thickness between 130 and 300 µm (Figure S1, Supporting Information), where titanium dioxide (TiO_2) is commonly embedded in the polymer resin as a white pigment.[22] However, TiO_2, known for its UV absorbing ability, introduces UV light into the polymer resin, causing photodegradation[23] and leaving a yellowish appearance after long-term exposure. Visible and near-infrared light can also contribute to the weathering of polymers, but UV radiation remains the most critical factor in radiation-induced weathering and is therefore the primary focus of this study. A hierarchically porous poly(vinylidene fluoride-co-hexafluoropropene) (P(VDF-HFP)) coating with nanoscale and microscale air pores has also been developed for radiative cooling (Case 2).[8] Although the porous P(VDF-HFP) coating demonstrates high solar reflectance, high thermal emittance, and outstanding UV resistance, its broader implementation is limited by its considerable cost of over ≈\$2.5 m^{-2}.[24]

To address the challenge of balancing between high radiative cooling performance with material costs, here we propose a cost-effective bilayer polymer paint (Case 3). This innovative design consists of a top layer of porous P(VDF-HFP), which enhances UV resistance and solar reflectance, and a bottom layer of commercial acrylic latex paint (ALP). The resulting bilayer paint exhibits a synergistic combination of properties: relatively high cooling performance, moderate material cost, and excellent UV durability. These characteristics render it a more viable candidate for real-world implementation of radiative cooling solutions.

2. Results and Discussion

2.1. Working Principle of the Bilayer Design

The development of efficient and cost-effective materials for radiative cooling applications has prompted researchers to explore innovative combinations of existing materials. P(VDF-HFP) is known for its high performance in terms of sunlight resistance, mechanical strength, and thermal stability,[25] making it an excellent choice for radiative coolers. However, its high cost restricts widespread adoption. To address this challenge, we propose a bilayer design (**Figure 2a**) that combines the strengths of both materials. By creating a composite structure with a porous P(VDF-HFP) layer for high performance and an ALP layer for cost-effectiveness, this approach aims to strike a balance between functionality and affordability.

Given the relatively short wavelength of UV radiation within the solar spectrum, a thin layer of porous P(VDF-HFP) has been proven to be sufficient for effective backscattering and high reflectance at UV wavelengths without significantly increasing material costs (Figure 2b). Meanwhile, the longer wavelengths passing through the thin P(VDF-HFP) layer, such as visible and near-infrared light at 0.7–1.5 µm, can be intercepted and reflected by the thicker bottom ALP layer (Figure 2b). The remaining 1.5–2.5 µm band in the solar spectrum is of lower significance due to its limited contribution. By integrating the two layers, this innovative bilayer design has the potential for large-scale implementation by balancing performance and cost-effectiveness.

The bilayer paint was fabricated by blade-coating a thin layer of P(VDF-HFP) onto a brush-coated ALP base, as shown in

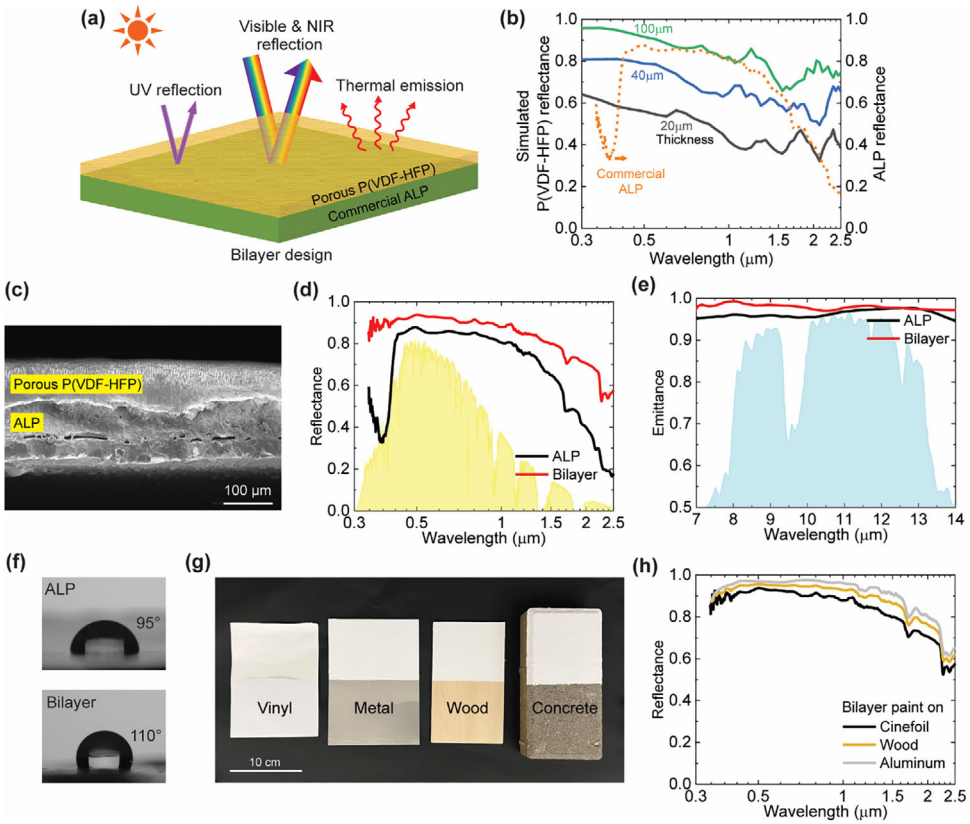

Figure 2. Working principle of the bilayer polymer paint. a) Schematic illustrating the interaction between the proposed bilayer paint and solar and thermal radiation. b) Simulated reflectance of a single P(VDF-HFP) layer at multiple thicknesses, indicating that its reflective capability decreases from UV to near-infrared wavelengths. c) SEM image showing the cross-section of the bilayer paint on a cinefoil substrate. d) Reflectance spectra of commercial ALP and the bilayer paint, highlighting enhancements in the UV wavelengths and across the entire solar spectrum. e) Emittance spectra of commercial ALP and the bilayer paint, with the atmospheric transmittance window plotted for reference. f) The water contact angle of the ALP base and the bilayer paint. The bilayer paint retains a hydrophobic surface due to the top P(VDF-HFP) layer. g) Demonstration of the bilayer paint applied to various substrate materials such as vinyl, metal, wood, and concrete. h) Reflectance spectra of the bilayer paint on different substrates, ranging from 0.89 on cinefoil to 0.95 on aluminum.

the cross-sectional scanning electron microscope (SEM) image (Figure 2c). The ALP layer exhibits a dense structure, while the P(VDF-HFP) layer contains air pores formed via phase inversion. Some pores in the porous P(VDF-HFP) layer appear slightly distorted due to shear stress during sample cross-sectioning. Compared to the original ALP layer, which has a thickness of ≈130 μm, the bilayer paint with a 99 μm thick P(VDF-HFP) layer demonstrates an enhanced solar reflectance, increasing from 0.78 to 0.89 (Figure 2d). This improvement is particularly notable in the UV reflectance range of 300–400 nm, which rises from 0.41 to 0.89 due to photon scattering at the nanoscale pores. Additionally, the microscale pores in the bilayer paint contribute to increased reflectance in the near-infrared spectrum.

Beyond optical properties within the solar spectrum, both the ALP and the bilayer paint exhibit high thermal emittance in the 7–14 μm range (Figure 2e), attributed to the intrinsic vibrational modes of the polymer molecules.[26,27] The bilayer paint shows a slightly higher thermal emittance, increasing from 0.96 to 0.98. Such high thermal emittance remains reliable under varying temperature conditions worldwide, due to the persistence of dominant vibrational modes and the presence of a porous structure (Figure S2, Supporting Information). The incorporation of the P(VDF-HFP) layer provides enhanced UV resistance and improves overall solar reflectance while maintaining high thermal emittance, resulting in better radiative cooling performance (Figure S3, Supporting Information).

Thanks to the hydrophobic property of P(VDF-HFP), the bilayer paint retains its hydrophobicity with a water contact angle of ≈110°, ensuring a self-cleaning capability (Figure 2f, Figure S4 and Video S1, Supporting Information). Notably, the bilayer paint can be applied onto various substrates (Figure 2g), offering versatility across multiple applications. Here, cinefoil was selected as the substrate (Figure 2c) due to its near-perfect blackbody property, which provides a non-reflective background. If other substrate materials such as wood or aluminum are used, the solar reflectance can be further improved to 0.92 and 0.95, respectively (Figure 2h; Figure S5, Supporting Information).

2.2. Reflectance Optimization by Tuning Pore Geometry

To enhance and optimize the solar reflectance of the bilayer paint, precise control over nano- and micro-pore distribution

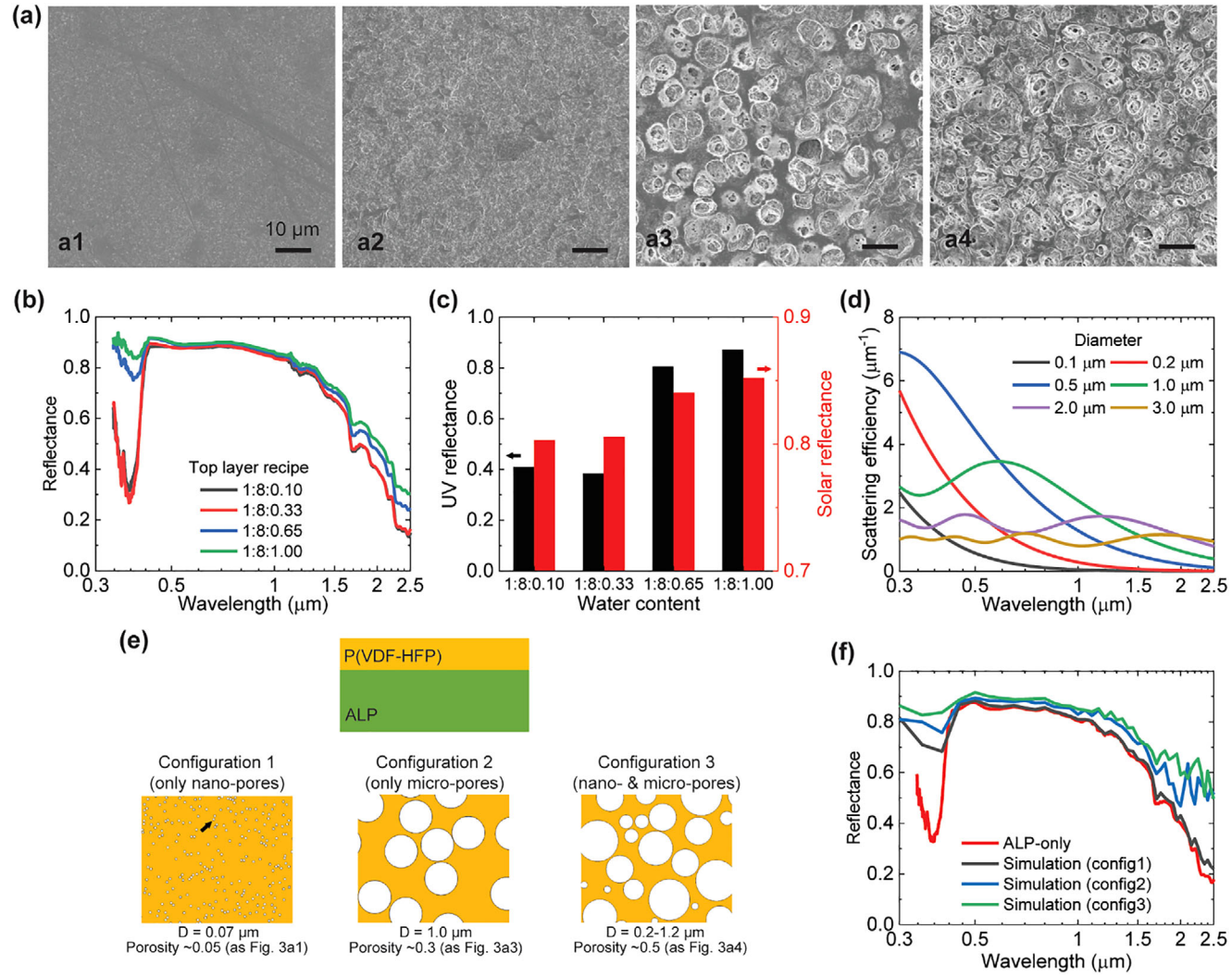

Figure 3. Reflectance optimization via pores. a) SEM images of the bilayer paint morphology with P(VDF-HFP):acetone:water weight ratios of (a1) 1:8:0.10, (a2) 1:8:0.33, (a3) 1:8:0.65, and (a4) 1:8:1.00. b) Reflectance spectra of the bilayer paint with different top layer recipes for the porous P(VDF-HFP), with the top layer thickness fixed at ≈38 μm. c) Corresponding UV reflectance and solar reflectance as different water contents. d) Independent scattering efficiency of air pores as a function of pore size within the P(VDF-HFP) matrix. e) Three configurations of COMSOL reflectance simulations. One contains only nano-pores, another contains only micro-pores, while the third contains both nano- and micro-pores. f) Reflectance simulation results as compared to the ALP base. A broader pore size distribution enhances reflectance across the entire solar spectrum.

is essential, as their arrangement significantly affects sunlight photon scattering efficiency. Pore control is primarily achieved through the chemical composition, or "recipe", during the phase inversion process under natural drying conditions. P(VDF-HFP) powder was dissolved in acetone and water at various P(VDF-HFP):acetone:water weight ratios from 1:8:0.10 to 1:8:1.00. A higher water content leads to flocculent insoluble of the P(VDF-HFP) component (Figure S6, Supporting Information). The use of acetone may enhance the binding force between the two layers, as it can dissolve the acrylic components in the ALP.

The resulting P(VDF-HFP) coatings exhibit morphologies ranging from dense structures (**Figure** 3a1) to hierarchically porous ones (Figure 3a4). Notably, the 1:8:1.00 composition displays the broadest size distribution of air pores across multiple scales (Figure S7, Supporting Information), facilitating efficient scattering in the whole solar spectrum. By adjusting the water content, the porous structure of the P(VDF-HFP) layer can be fine-tuned to achieve the desired UV and solar reflectance properties (Figure 3b). With an optimized recipe, the UV reflectance of the bilayer paint is enhanced from 0.41 to 0.87, while overall solar reflectance increases from 0.80 to 0.85, achieved with a thin 38 μm P(VDF-HFP) layer (Figure 3c). Emittance measurements indicate high thermal emittance (>0.96) across all formulations (Figure S8, Supporting Information), as both ALP and P(VDF-HFP) serve as effective thermal emitters.

To investigate the effects of hierarchically sized pores on solar reflectance enhancement, scattering efficiency was computed based on Mie scattering theory (Figure 3d). The results indicate that nano-pores are effective at scattering shorter wavelengths, while micro-pores are more effective at scattering longer wavelengths such as the near-infrared components in the sunlight. Thus, a broader pore size distribution encompassing

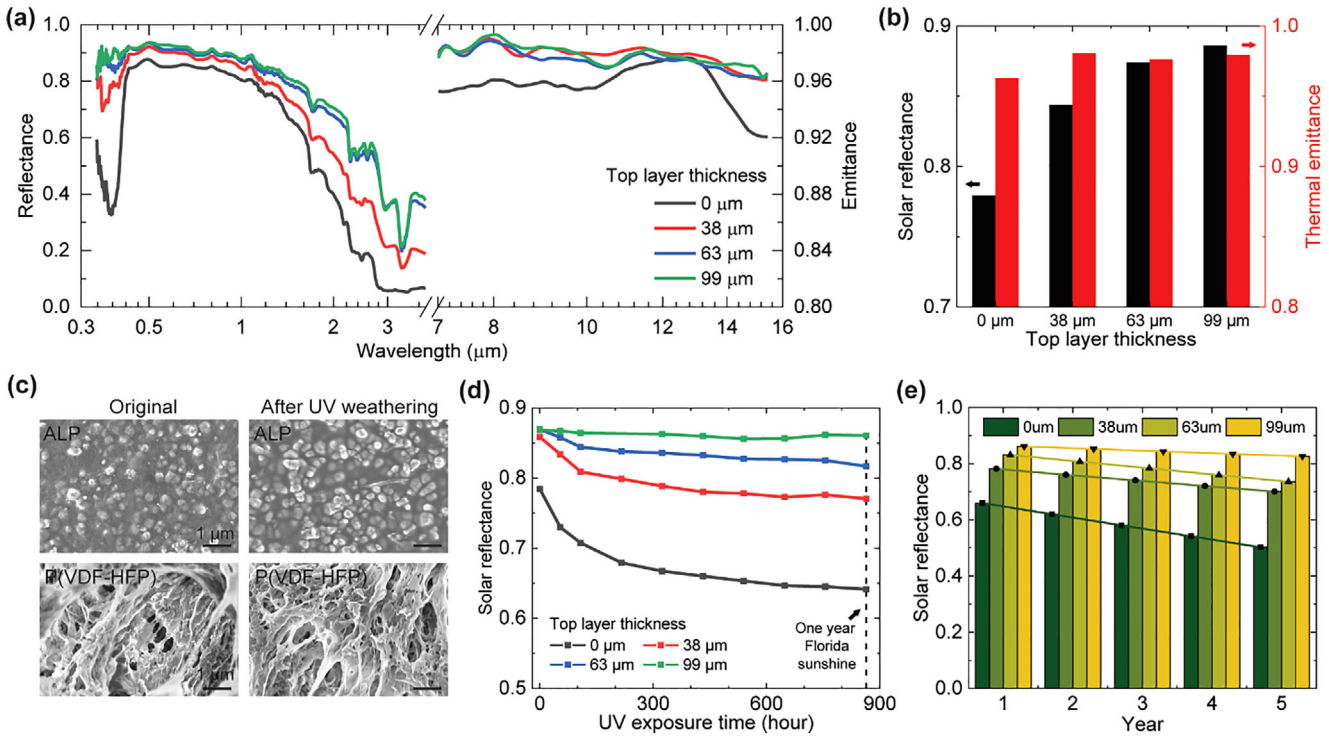

Figure 4. Reflectance optimization via thickness and UV degradation. a) Reflectance and emittance spectra of the bilayer paint with varying thicknesses of the P(VDF-HFP) top layer. b) Corresponding solar reflectance and thermal emittance as a function of the thickness of the P(VDF-HFP) layer. c) SEM images of ALP and P(VDF-HFP) before/after UV weathering, showed no obvious morphological changes. d) The solar reflectance of the bilayer paint is a function of UV exposure time. A UV dosage of 864 h is equivalent to one year of UV exposure in Florida, which amounts to ≈275 MJ m^{-2}.[31] e) Estimated solar reflectance of the bilayer paint over the years, extrapolated from the UV weathering results.

both nanoscale and microscale pores, as shown in Figure 3a4, is expected to enhance scattering and reflectance across the entire spectrum. To confirm this, reflectance simulations of three porous configurations were conducted using COMSOL (Figure 3e). One configuration contains only nano-pores with a diameter of 0.07 μm (as Figure 3a1), another contains only micro-pores with a diameter of 1.0 μm (as Figure 3a3), while the third includes both nano- and micro-pores ranging from 0.2 to 1.2 μm, resembling Figure 3a4. The simulation results validate the enhancements in UV and near-infrared reflectance achieved through the broader pore size distribution (Figure 3f).

2.3. Reflectance Optimization by Thickness and UV Degradation

Another approach to optimizing solar reflectance involves controlling the thickness of the P(VDF-HFP) layer. Multiple thicknesses of the P(VDF-HFP) layer were applied onto the ALP base through multiple rounds of blade coating. The solar reflectance results (**Figure** 4a) demonstrate that the porous P(VDF-HFP) layer enhances both UV and near-infrared reflectance, owing to its negligible extinction coefficient across the solar spectrum, in contrast to the ALP. At the top layer thicknesses of 38, 63, and 99 μm, the overall solar reflectance increases from 0.78 to 0.84, 0.87, and 0.89, respectively, while thermal emittance rises slightly from 0.96 to 0.98 (Figure 4b).

Although thicker porous P(VDF-HFP) layers perform better with higher solar reflectance, they also incur higher material costs; for example, a 300 μm thick layer achieves a solar reflectance of 0.96 and a thermal emittance of 0.97 at a cost of over ≈$2.5 m^{-2}.[8,24] Additionally, subsequent results from UV weathering tests indicate that a 99 μm thick P(VDF-HFP) layer already exhibits excellent UV durability. Therefore, the top layer thickness above 100 μm was not considered to ensure cost-effectiveness. The 99 μm thick P(VDF-HFP) layer with a material usage reduction of ≈70% achieves the optimal balance of high solar reflectance and thermal emittance.

The proposed bilayer paint is compared with other radiative cooling materials, both porous and non-porous, as summarized in Table S1 (Supporting Information). This design offers advantages in terms of low cost and scalability. For real-world implementation, the large-scale production of the bilayer paint usually involves roll-to-roll manufacturing, where roll coating is applied to the substrate, followed by a phase inversion drying process for the porous P(VDF-HFP) via spray coating. To ensure a uniform distribution of the porous structure and consistent coating thickness, it is crucial to carefully control processing parameters such as roll temperature, spray parameters (pressure, distance, angle, etc.), as well as ambient temperature and relative humidity.

As widely recognized, paint degrades over time due to exposure to extreme temperatures and sunlight in real-world implementation, necessitating refurbishment every 5–10 years.[28,29] To evaluate the cost-effectiveness of the proposed bilayer paint, its UV durability and service lifetime must be considered. In this study, we conducted a UV accelerated weathering test to assess

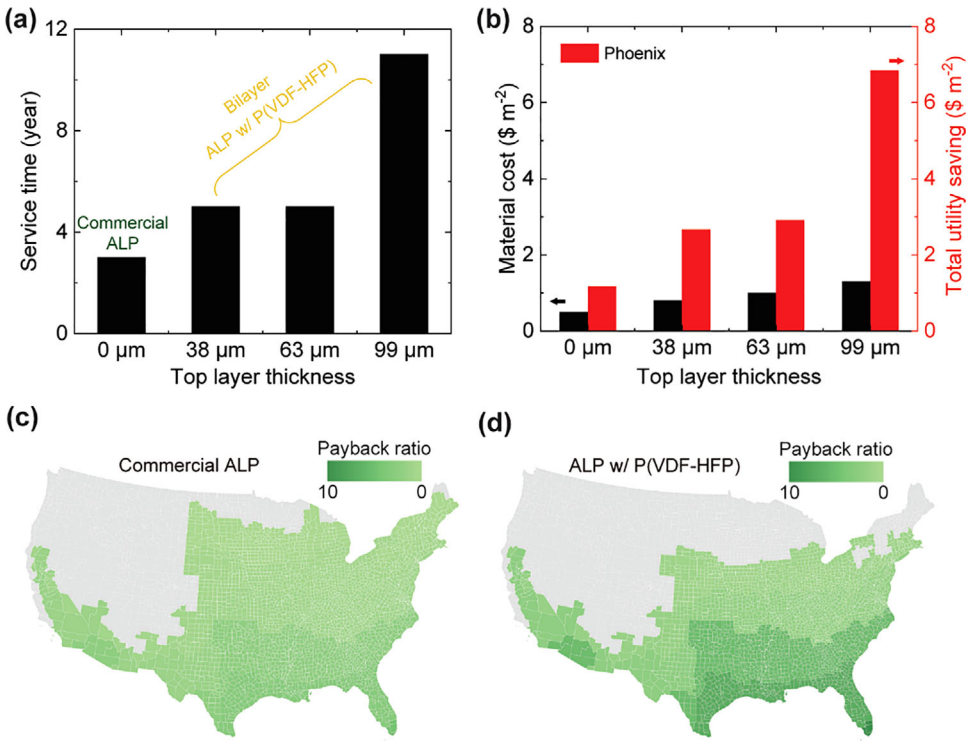

Figure 5. Energy savings over entire service lifetime. a) The service lifetime of the commercial ALP and the bilayer paint, with a threshold set at 0.9 for solar reflectance degradation. b) Material costs and total utility savings over service lifetime, using Phoenix as an example. c,d) Payback ratios for (c) the commercial ALP and (d) the bilayer paint, highlighting the cost-effectiveness of the bilayer design. The payback ratio is defined as the total utility saving over the entire service lifetime divided by the material cost.

the reliability of the bilayer paint. Samples with varying thicknesses of the P(VDF-HFP) layer were exposed to a UV dosage simulating one year of sunlight in Florida (see Experimental Section).

Although no obvious morphological changes were observed before and after UV weathering (Figure 4c), the solar reflectance of the bilayer paint samples decreased during the UV exposure. Specifically, the ALP-only sample's solar reflectance drops from 0.78 to 0.64, while the sample with a 99 μm thick P(VDF-HFP) layer exhibits minimal solar reflectance degradation that is less than 0.01 (Figure 4d). Meanwhile, the bilayer paints show negligible change (<0.04) in their thermal emittance after the UV weathering test (Figure S9, Supporting Information). In different regions worldwide, solar intensity and the proportion of UV radiation vary. Therefore, the thickness of the top P(VDF-HFP) layer should be tailored to local environmental conditions. Here, the AM1.5G solar spectrum and the Florida UV dosage (≈275 MJ m^{-2} per year) are used as references.

To analyze the paints' reliability in the long term, the solar reflectance over time was projected by extrapolating experimental data. The degradation of solar reflectance R_{solar} over time t is assumed to follow a model combining an exponentially decaying term and a linearly decreasing term,[30] as represented by the following equation:

$$R_{solar} = C_1 + C_2 e^{-C_3 t} - C_4 t \quad (1)$$

where C_1, C_2, C_3, and C_4 are fitting parameters to be determined. Using the UV weathering data, we extrapolate the solar reflectance over time (Figure 4e; Figure S10, Supporting Information). The results indicate that incorporating the P(VDF-HFP) top layer can markedly enhance the durability and extend the service life of the paints.

2.4. Economic Analysis

To evaluate the overall cost-effectiveness of the paint over its entire service lifetime, a threshold of 0.9 was set for solar reflectance degradation, indicating that the paint becomes underperforming and requires refurbishment once its reflectance drops to 90% of its initial value. Under this criterion, the commercial ALP has a service lifetime of only three years, while the bilayer paint can last between 5 and 11 years, depending on the thickness of the P(VDF-HFP) layer (**Figure 5a**).

Then we use a midrise apartment building—a commercial reference defined by the U.S. Department of Energy (DOE)—as an example (see Experimental Section). Assuming the paint is applied to the building rooftop to reject sunlight, we sequentially input the yearly degrading data of solar reflectance and a constant thermal emittance of 0.95 into EnergyPlus to simulate annual energy consumption over the years. By summing the energy savings over multiple years through the paint's service lifetime, we calculate the total utility saving compared to the original DOE template, where the roof exterior surface has a solar reflectance

of 0.30. The results for Phoenix are shown in Figure 5b, alongside the material costs (Figure S11, Supporting Information). Notably, the 99 μm thick P(VDF-HFP) layer increases the total utility saving by ≈6 fold, even though the associated material cost is only ≈2.6 times higher. This improvement is attributed to the extended service lifetime of the bilayer paint with excellent UV resistance.

Furthermore, we define a payback ratio as a figure of merit for cost-effectiveness:

$$\text{Payback ratio} = \frac{\text{Total utility saving}}{\text{Material cost}} \quad (2)$$

The maps across the United States for the ALP (Figure 5c) and the proposed bilayer paint (Figure 5d) reveal an enhanced payback ratio for the proposed design, increasing from up to 4.5 to as high as 10.1 when used as a radiative cooling paint on building roofs. It is noteworthy that in the northern U.S., the payback ratio is negative due to the heating penalty in winter, which outweighs cooling benefits. Therefore, with the introduced P(VDF-HFP) top layer, the bilayer paint not only reduces the frequency of refurbishments but also delivers significant energy savings in warm areas, featuring much higher cost-effectiveness. Additionally, it is worth noting that the choice of substrate can affect not only the cooling performance due to background reflectance, but also the cost-effectiveness due to potential substrate aging issues (e.g., metal corrosion, concrete cracking), which warrants further investigation in the future.

2.5. Additional Environmental Factors and Mechanical Durability

In real-world conditions, the bilayer polymer paint is subjected to various environmental aging factors in addition to UV radiation, including acid rain, mud soiling, temperature, humidity, and icing. To evaluate the paint's durability, these aging tests were conducted (see Experimental Section), and the samples were assessed before and after exposure using solar reflectance, thermal emittance, water contact angle, and sliding angle as performance metrics (Figure S12 and Table S2, Supporting Information).

The temperature, humidity, acid rain, and icing aging tests decrease the bilayer paint's water contact angle and increase its sliding angle, but the bilayer paint still possesses a water contact angle >≈100°, demonstrating adequate hydrophobicity. Thus, the mud on the bilayer paint can roll off spontaneously, and the dust can be easily carried away by water without any residue (Figure S4 and Video S1, Supporting Information). To synergistically evaluate the aging effects of these factors together, a 14-day outdoor exposure test was performed. The bilayer paint exhibits better environmental resistance than the ALP, along with greater hydrophobicity and more favorable optical properties.

Besides the aging effect, it is worth noting that the humidity may affect the pore structure of the top P(VDF-HFP) layer during on-site implementation, which requires customization based on local weather conditions. It may also influence cooling performance, as increased humidity reduces sky transparency. Additionally, since the bilayer polymer coating is primarily intended for use in warm regions for cooling purposes, potential issues related to icing or frosting[32] are not expected to be a concern.

Furthermore, to evaluate the mechanical durability of the bilayer paint, cross-cut tape, dry abrasion, and sand falling abrasion tests were conducted (see Experimental Section). The bilayer paint exhibits 3B-level adhesion (Figure S13, Supporting Information), lower than the ALP's 5B level due to its porous structure, but still satisfies the paint adhesion requirement for wall and ceiling coatings for exterior use according to the Green Seal Standard GS-11,[33] which applies to both commercial and residential buildings. The dry abrasion test using steel wool and the sand falling abrasion test damaged the bilayer paint surface (Figure S14, Supporting Information), leading to a lower water contact angle and a higher sliding angle (Figure S12, Supporting Information). However, the bilayer paint still outperforms the original ALP in these rubrics. Last but not least, the optical properties of the bilayer paint are barely affected by the aging tests (Figure S12, Supporting Information), ensuring its cooling performance during the service lifetime.

3. Conclusion

In this work, we developed a cost-effective bilayer polymer paint for radiative cooling applications, combining a porous P(VDF-HFP) top layer with a commercial ALP base. Through precise control of nano- and micro-pore distribution in the P(VDF-HFP) layer, we optimized solar reflectance and UV resistance. The bilayer paint demonstrated enhanced UV reflectance from 0.41 to 0.89 and increased overall solar reflectance from 0.78 to 0.89 with a thin P(VDF-HFP) layer.

UV accelerated weathering tests revealed superior durability of the bilayer paint compared to ALP alone, with minimal solar reflectance degradation over simulated long-term exposure. Using a degradation model, we projected service lifetimes of 5–11 years for the bilayer paint, significantly outperforming the 3-year lifespan of commercial ALP. Cost-effectiveness analysis, based on EnergyPlus simulations for a midrise apartment building, demonstrated that the bilayer paint with a 99 μm P(VDF-HFP) layer increased total utility savings ≈6 fold while increasing material costs only by 2.6 times. The introduced payback ratio metric revealed enhanced cost-effectiveness across the United States, with values up to 10.1 for the bilayer paint compared to 4.5 for the ALP.

These findings highlight the potential of our bilayer polymer paint as a practical and economically viable solution for large-scale implementation of radiative cooling. By addressing key challenges in performance, durability, and cost-effectiveness, this innovative design paves the way for sustainable cooling solutions in a warming world, offering significant energy savings and reduced environmental impact in warm climates.

4. Experimental Section

Materials: The P(VDF-HFP) powder (Kynar Flex 2801) was obtained from Arkema. Acetone and deionized water were purchased from Thermo Scientific Chemicals. The acrylic latex paint (SW7757 High Reflective White) was purchased from Sherwin–Williams. The substrate used was Rosco matte cinefoil purchased from Amazon. Silica sand (Teton Supply Co., 120 mesh) was purchased from Amazon. Steel wool of grade #0000 was purchased from Home Depot. Hydrochloric acid was purchased from Sigma–Aldrich.

Fabrication and SEM Imaging of the Bilayer Paint: The acrylic latex paint was brush-coated onto the cinefoil substrate, an ideal blackbody, which was selected to provide a non-reflective background. After air-drying in a fume hood for 12 h, a porous P(VDF-HFP) layer was formed by blade-coating a pre-mixed solution of P(VDF-HFP), acetone, and water at a specific weight ratio. A thicker P(VDF-HFP) layer was achieved through additional rounds of blade coating. A P(VDF-HFP):acetone:water weight ratio 1:8:1.00 yielded the highest solar reflectance. SEM imaging was performed using a Zeiss Sigma VP SEM at an operating voltage of 4 kV.

Optical Characterization: The reflectance was determined separately in four wavelength bands: 0.337–0.43 µm, 0.43–1.1 µm, 1.1–2.5 µm, and 2.5–15.4 µm. In the first band (0.337–0.43 µm), the reflectance was measured using a near UV LED light array coupled to a PTFE integrating square and an Ocean Optics STS-VIS spectrophotometer. In the second band (0.43–1.1 µm), measurements were taken with an integrating sphere (Thorlabs IS200) and a high-power supercontinuum laser (SuperK Extreme, NKT Photonics) coupled with a tunable bandpass filter (Fianium LLTF contrast). The third and fourth spectra (near-infrared and mid-infrared) were measured using a Fourier Transform Infrared spectrometer (Bruker Vertex 70v) and a gold integrating sphere (Labsphere 4P-GPS-020-SL) along with a mercury cadmium telluride detector. The four reflectance spectra were patched together.

Solar reflectance R_{solar} and emittance ϵ were calculated using the following equations. $I_{AM1.5G}$ represents the air mass 1.5G solar spectrum, R is the reflectance spectrum, and I_{bb} is the spectral blackbody radiance at temperature T (assumed at 20 °C) according to Planck's law.

$$R_{solar} = \frac{\int_{0.3\,\mu m}^{2.5\,\mu m} I_{AM1.5G}(\lambda)\, R(\lambda)\, d\lambda}{\int_{0.3\,\mu m}^{2.5\,\mu m} I_{AM1.5G}(\lambda)\, d\lambda} \quad (3)$$

$$\epsilon(\lambda) = 1 - R(\lambda) \quad (4)$$

$$\epsilon_{\lambda_1 to \lambda_2}(T) = \frac{\int_{\lambda_1}^{\lambda_2} I_{bb}(\lambda, T)\, \epsilon(\lambda)\, d\lambda}{\int_{\lambda_1}^{\lambda_2} I_{bb}(\lambda, T)\, d\lambda} \quad (5)$$

COMSOL Reflectance Simulation: The 2D full-field electromagnetic simulations[34] were performed to model the reflectance of the bilayer paint. Nano- and micro-pores were randomly distributed within the P(VDF-HFP) layer. A plane wave was excited above the material, with periodic boundary conditions applied to the left and right sides. Light intensity was monitored at two ports positioned on the top and bottom sides of the material, which were integrated to obtain reflectance and transmittance values.

UV Weathering Test: Q-LAB QUV Accelerated Weathering Tester equipped with UVA-340 lamps was used to expose the prepared paint samples of 2 "x2" to UV light at 60 °C for 54, 108, 216, 324, 432, 540, 648, 756, and 864 h. The lamp intensity was 1.55 W m^{-2} nm^{-1} at 340 nm, resulting in a total UV intensity of 88.43 W m^{-2} based on the irradiance spectrum provided by the lamp manufacturer. Thus, 864 h of UV exposure corresponds to an accumulated dose of ≈275 MJ m^{-2}, simulating one year of sunlight in Florida.[31]

Additional Environmental Aging Tests and Mechanical Durability Tests: The paint samples were heated at 80 °C for 14 days as an accelerated thermal aging test, exposed to 100% relative humidity for 14 days as a humidity aging test, and immersed in an HCl solution (pH = 4.5) for 14 days to mimic an acid rain aging test, and subjected to 10 full icing-deicing cycles as an icing aging test. Moreover, the paint samples were exposed outdoors on a building roof at 40.4701° N, 86.9460° W for 14 days with adequate sunshine and occasional rain.

The adhesion of the paint samples was tested using a cross-cut tape test following ASTM D3359-23. The dry abrasion resistance of the paint samples was tested using steel wool for 2000 cycles following ASTM D8380-21. In the sand falling abrasion test, sand of 120 mesh (≈125 µm), with a total mass of 2000 g, was dropped from a height of ≈30 cm onto the paint samples which were tilted at 45°. The water contact angle and sliding angle were analyzed using an Ossila contact angle goniometer.

EnergyPlus Modeling: The building model used was the post-1980 midrise apartment building defined by the U.S. Department of Energy (DOE).[35] The U.S. was divided into 16 climate zones according to the International Energy Conservation Code, with 16 cities chosen to represent each zone: Miami (1A), Houston (2A), Phoenix (2B), Atlanta (3A), Los Angeles (3B), San Francisco (3C), Baltimore (4A), Albuquerque (4B), Seattle (4C), Chicago (5A), Boulder (5B), Minneapolis (6A), Helena (6B), Duluth (7A), Jackson (7B), and Fairbanks (8). In each city-specific simulation, the roof's solar reflectance was set to the yearly values extrapolated from the experimental UV weathering data. Simulations covered the paint's entire service lifetime, with each year's degraded solar reflectance calculated in sequence and summed for total energy impact. For example, the ALP case required a three-year simulation, while the case of 99 µm thick P(VDF-HFP) top layer required an eleven-year simulation. Energy savings in natural gas and electricity were determined by comparing these cases to the original DOE reference with a roof solar reflectance of 0.30. Utility savings were calculated using a natural gas rate of $0.95 per therm and an electricity rate of $0.164 per kWh.

Supporting Information

Supporting Information is available from the Wiley Online Library or from the author.

Acknowledgements

Y.Y. acknowledges support from the National Science Foundation (Award No. 2005747) and the Urban Tech Award from Columbia University.

Conflict of Interest

The authors declare no conflict of interest.

Author Contributions

The idea is conceived by Q.C. and Y.Y. Sample preparation, material characterization, and optical measurements are performed by Q.C. and C.T. UV weathering tests are conducted by B.W.K. Economic analysis, additional aging tests, and mechanical durability tests are carried out by Q.C. Reflectance measurements are supported by Y.X. The project is supervised by Q.C. and Y.Y. All authors contribute to the writing of the paper.

Data Availability Statement

The data that support the findings of this study are available from the corresponding author upon reasonable request.

Keywords

bilayer, polymer paint, porous structure, radiative cooling, UV degradation

Received: March 11, 2025
Revised: May 10, 2025
Published online:

[1] S. Perkins-Kirkpatrick, D. Barriopedro, R. Jha, L. Wang, A. Mondal, R. Libonati, K. Kornhuber, *Nat. Rev. Earth Environ.* **2024**, *5*, 244.

[2] E. Scoccimarro, O. Cattaneo, S. Gualdi, F. Mattion, A. Bizeul, A. M. Risquez, R. Quadrelli, *Commun. Earth Environ.* **2023**, *4*, 208.
[3] K. Lundgren-Kownacki, E. D. Hornyanszky, T. A. Chu, J. A. Olsson, P. Becker, *Int. J. Biometeorol.* **2017**, *62*, 401.
[4] A. P. Raman, M. A. Anoma, L. Zhu, E. Rephaeli, S. Fan, *Nature* **2014**, *515*, 540.
[5] M. Lee, G. Kim, Y. Jung, K. R. Pyun, J. Lee, B.-W. Kim, S. H. Ko, *Light: Sci. Appl.* **2023**, *12*, 134.
[6] J. He, Q. Zhang, Y. Zhou, Y. Chen, H. Ge, S. Tang, *ACS Nano* **2024**, *18*, 11120.
[7] D. Li, X. Liu, W. Li, Z. Lin, B. Zhu, Z. Li, J. Li, B. Li, S. Fan, J. Xie, J. Zhu, *Nat. Nanotechnol.* **2020**, *16*, 153.
[8] J. Mandal, Y. Fu, A. C. Overvig, M. Jia, K. Sun, N. N. Shi, H. Zhou, X. Xiao, N. Yu, Y. Yang, *Science* **2018**, *362*, 315.
[9] T. Li, Y. Zhai, S. He, W. Gan, Z. Wei, M. Heidarinejad, D. Dalgo, R. Mi, X. Zhao, J. Song, J. Dai, C. Chen, A. Aili, A. Vellore, A. Martini, R. Yang, J. Srebric, X. Yin, L. Hu, *Science* **2019**, *364*, 760.
[10] J. Li, Y. Liang, W. Li, N. Xu, B. Zhu, Z. Wu, X. Wang, S. Fan, M. Wang, J. Zhu, *Sci. Adv.* **2022**, *8*, abj9756.
[11] X. Zhao, T. Li, H. Xie, H. Liu, L. Wang, Y. Qu, S. C. Li, S. Liu, A. H. Brozena, Z. Yu, J. Srebric, L. Hu, *Science* **2023**, *382*, 684.
[12] K. Lin, S. Chen, Y. Zeng, T. C. Ho, Y. Zhu, X. Wang, F. Liu, B. Huang, C. Y.-H. Chao, Z. Wang, C. Y. Tso, *Science* **2023**, *382*, 691.
[13] X. Yan, M. Yang, W. Duan, H. Cui, *ACS Nano* **2024**, *18*, 27752.
[14] Z. Chen, S. Yu, J. Ma, B. Xie, S.-K. Kim, R. Hu, *Fundam. Res.* **2025**, https://doi.org/10.1016/j.fmre.2024.12.019.
[15] C. Lin, K. Li, M. Li, B. Dopphoopha, J. Zheng, J. Wang, S. Du, Y. Li, B. Huang, *Adv. Mater.* **2024**, https://doi.org/10.1002/adma.202409738.
[16] J. Mandal, Y. Yang, N. Yu, A. P. Raman, *Joule* **2020**, *4*, 1350.
[17] Q. Gong, L. Lu, J. Chen, W. Y. Lau, K. H.o Cheung, *Sol. Energy* **2023**, *255*, 236.
[18] X. Xue, M. Qiu, Y. Li, Q. M. Zhang, S. Li, Z. Yang, C. Feng, W. Zhang, J. G. Dai, D. Lei, W. Jin, L. Xu, T. Zhang, J. Qin, H. Wang, S. Fan, *Adv. Mater.* **2020**, *32*, 1906751.
[19] A. Mastrucci, E. Byers, S. Pachauri, N. D. Rao, *Energy Build.* **2019**, *186*, 405.
[20] R. Khosla, N. D. Miranda, P. A. Trotter, A. Mazzone, R. Renaldi, C. McElroy, F. Cohen, A. Jani, R. Perera-Salazar, M. McCulloch, *Nat. Sustain.* **2020**, *4*, 201.
[21] M. Honegger, A. Michaelowa, J. Pan, *Mitig. Adapt. Strateg. for Global Change* **2021**, *26*, 21.
[22] M. P. Diebold, *J. Coat. Technol. Res.* **2019**, *17*, 1.
[23] K. Wojciechowski, E. Skowera, E. Pietniewicz, G. Z. Zukowska, L. G. J. van der Ven, I. Korczagin, P. Malanowski, *Prog. Org. Coat.* **2014**, *77*, 298.
[24] Y. Yang, Y. Zhang, *MRS Energy Sustain.* **2020**, *7*, 1.
[25] M. R. Islam, G. Tudryn, R. Bucinell, L. Schadler, R. C. Picu, *Sci. Rep.* **2017**, *7*, 13070.
[26] G. Duan, C. Zhang, A. Li, X. Yang, L. Lu, X. Wang, *Nanoscale Res. Lett.* **2008**, *3*, 118.
[27] Y. Bormashenko, R. Pogreb, O. Stanevsky, E. Bormashenko, *Polym. Test.* **2004**, *23*, 791.
[28] J. L. Dias, A. Silva, C. Chai, P. L. Gaspar, J. de Brito, *Building Res. Info.* **2013**, *42*, 371.
[29] X. He, W. Zhou, *Sci. Rep.* **2024**, *14*, 30174.
[30] L. A. Gavrilov, N. S. Gavrilova, *Handbook of the Biology of Aging*, Academic Press, Cambridge, MA, USA, **2005**, p. 3.
[31] M. Sleiman, T. W. Kirchstetter, P. Berdahl, H. E. Gilbert, S. Quelen, L. Marlot, C. V. Preble, S. Chen, A. Montalbano, O. Rosseler, H. Akbari, R. Levinson, H. Destaillats, *Sol. Energy Mater. Sol. Cells* **2014**, *122*, 271.
[32] S. Yang, Q. Li, B. Du, Y. Ying, Y. Zeng, Y. Jin, X. Qin, S. Gao, S. Wang, Z. Wang, R. Wen, X. Ma, *Int. J. Extreme Manuf.* **2023**, *5*, 045501.
[33] Green Seal. GS-11 Paints, Coatings, Stains, And Sealers, https://greenseal.org/standards/gs-11-paints-coatings-stains-and-sealers/.
[34] M. Chen, D. Pang, J. Mandal, X. Chen, H. Yan, Y. He, N. Yu, Y. Yang, *Nano Lett.* **2021**, *21*, 1412.
[35] M. Deru, K. Field, D. Studer, K. Benne, B. Griffith, P. Torcellini, B. Liu, M. Halverson, D. Winiarski, M. Rosenberg, *US Department of Energy Commercial Reference Building Models of the National Building Stock*, National Renewable Energy Laboratory, Golden, CO, USA **2011**, 1.